

1 **Geophysical surveys to help map buried igneous intrusions, Snowdonia,**

2 **North Wales, UK**

3

4 Moseley, D.P.^{1,2}, Pringle, J.K.^{1*}, Haslam, R.B.^{1,3}, Egan, S.S.¹, Rogers, S.L.¹,

5 Gertisser, R.¹, Cassidy, N.J.¹ & Stimpson, I.G.¹

6

7 ¹School of Physical and Geographical Sciences, Keele University, Keele,

8 Staffordshire, ST5 5BG, U.K.

9

10 ²Hannon Westwood, 8 Old Lodge Place, St. Margaret's, Twickenham,

11 Middlesex, TW1 1RQ, U.K.

12

13 ³British Geological Survey, Environmental Science Centre, Nicker Hill,

14 Keyworth, Nottingham, NG12 5GG, U.K.

15

16 *contact email: j.k.pringle@keele.ac.uk

17

18

19 **Abstract**

20

21 The geology of the Snowdonia National Park in North Wales comprises a
22 mixture of Lower Palaeozoic shallow marine sediments, acidic igneous rocks
23 and basic intrusions of the Welsh Basin that were subsequently deformed during
24 the Caledonian Orogeny. Thin igneous intrusions are challenging to map due to
25 variable surface exposures, their intrusive origin, structural deformation and
26 burial by glacial sediments. This study used a combination of traditional
27 geological techniques, near-surface geophysical surveys and remote sensing to
28 detect and map a buried dolerite sheet intrusion. Both simple and mathematical
29 analysis of magnetic anomalies and numerical modelling allowed the dolerite
30 position, depths and target widths to be determined. Results showed that
31 calibrated magnetic surveys can characterise buried igneous bodies in such
32 mountainous environments.

33

34

35 **Introduction**

36

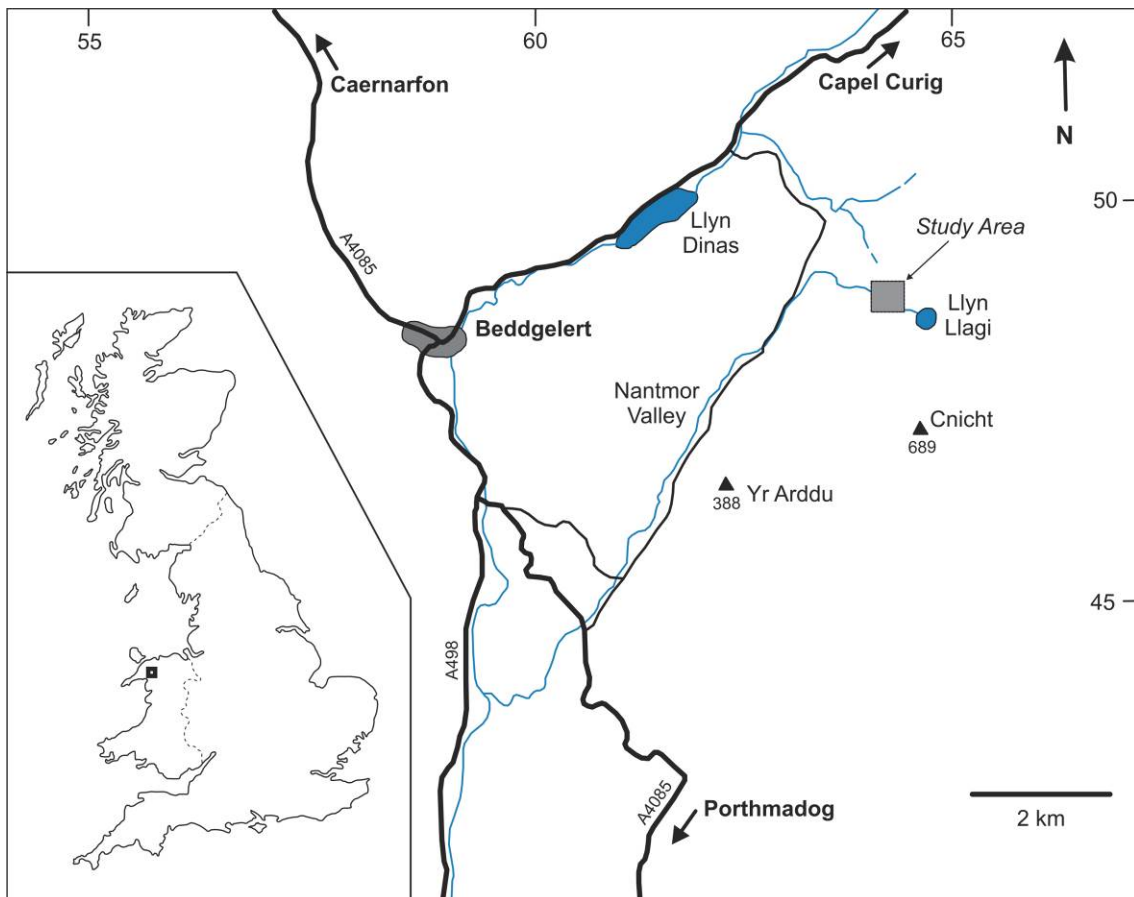
37 For geologists, standard field mapping of exposed geology and obtaining
38 sedimentary and structural data is critical to provide a geological map, cross
39 section and geological history of a field area. It is also important to map buried
40 geology where exposures are more variable. Remote sensing imagery analysis
41 can aid with this but often cannot provide high resolution of both the location the
42 identification of buried geology.

43

44 Near-surface geophysical surveys can detect, characterise and estimate the
45 depth of buried bedrock geology. Modern geophysical survey methods can also
46 be rapidly undertaken and cover large areas in short time frames. Magnetic
47 surveys have been very effective to map buried bedrock geology, provided there
48 is a sufficient contrast in magnetic susceptibility between the target and
49 background rocks. The overlying sediment deposits also need not to be too
50 thick. Bulk ground electro-magnetic (EM) conductivity surveys can also map
51 contrasting rock types and associated boundaries. Seismic surveys have been
52 used to map buried bedrock depth but suffer from poor resolution and would be
53 logistically difficult to collect in such environments. Ground Penetrating Radar
54 (GPR) surveys suffer from limited penetration depths. Lastly, microgravity
55 datasets have been used to map buried bedrock geology but need significant
56 rock density contrasts and is difficult to acquire in mountainous terrain.

57

58 This paper shows how traditional geological mapping, remote sensing and near-
59 surface geophysics can create a detailed map of partially buried geology in
60 mountainous terrain in the Snowdonia National Park in North Wales (**Fig. 1**).
61 This also included determining the extent of a dolerite sheet intruded into older
62 sedimentary and acidic volcanic rocks, all of which were partially buried by
63 glacial deposits. Near-surface geophysical surveys were also collected to test
64 their suitability and effectiveness. Lastly, simple and numerical analysis and
65 numerical modelling were combined to determine likely target depths and
66 widths.



67

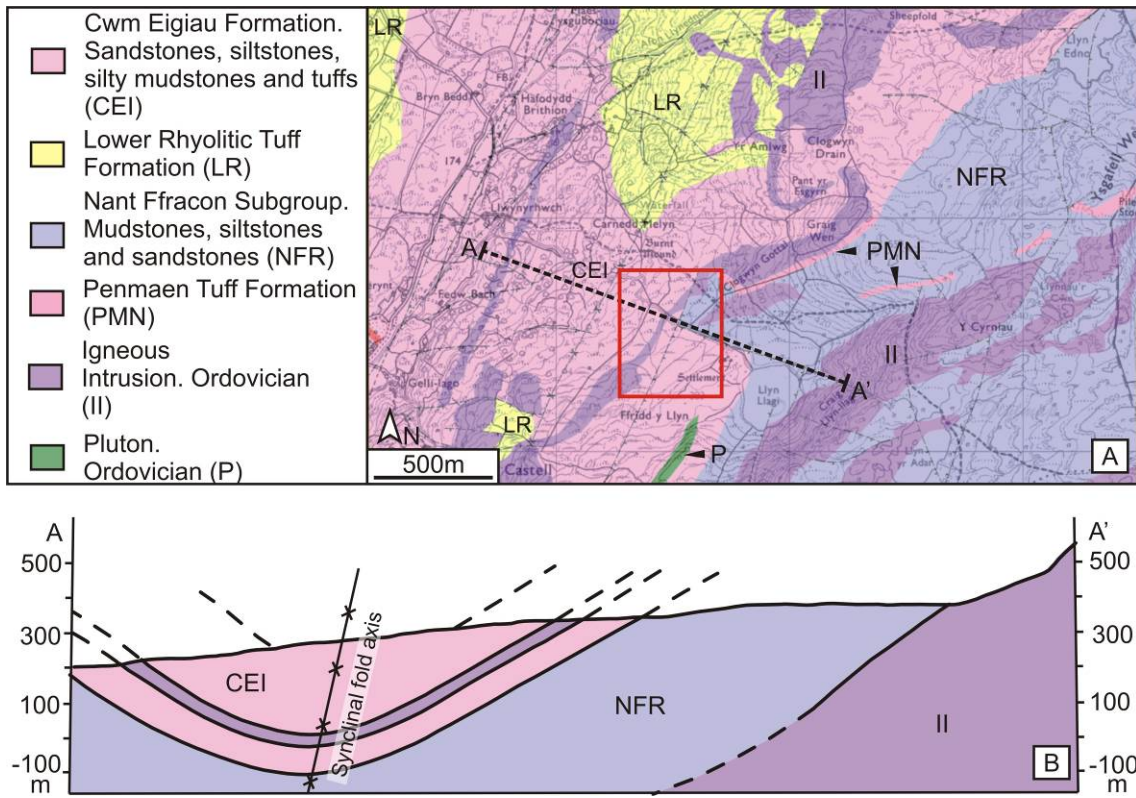
68 **Fig. 1.** Location map of the study area (boxed) with U.K. location map (inset).

69

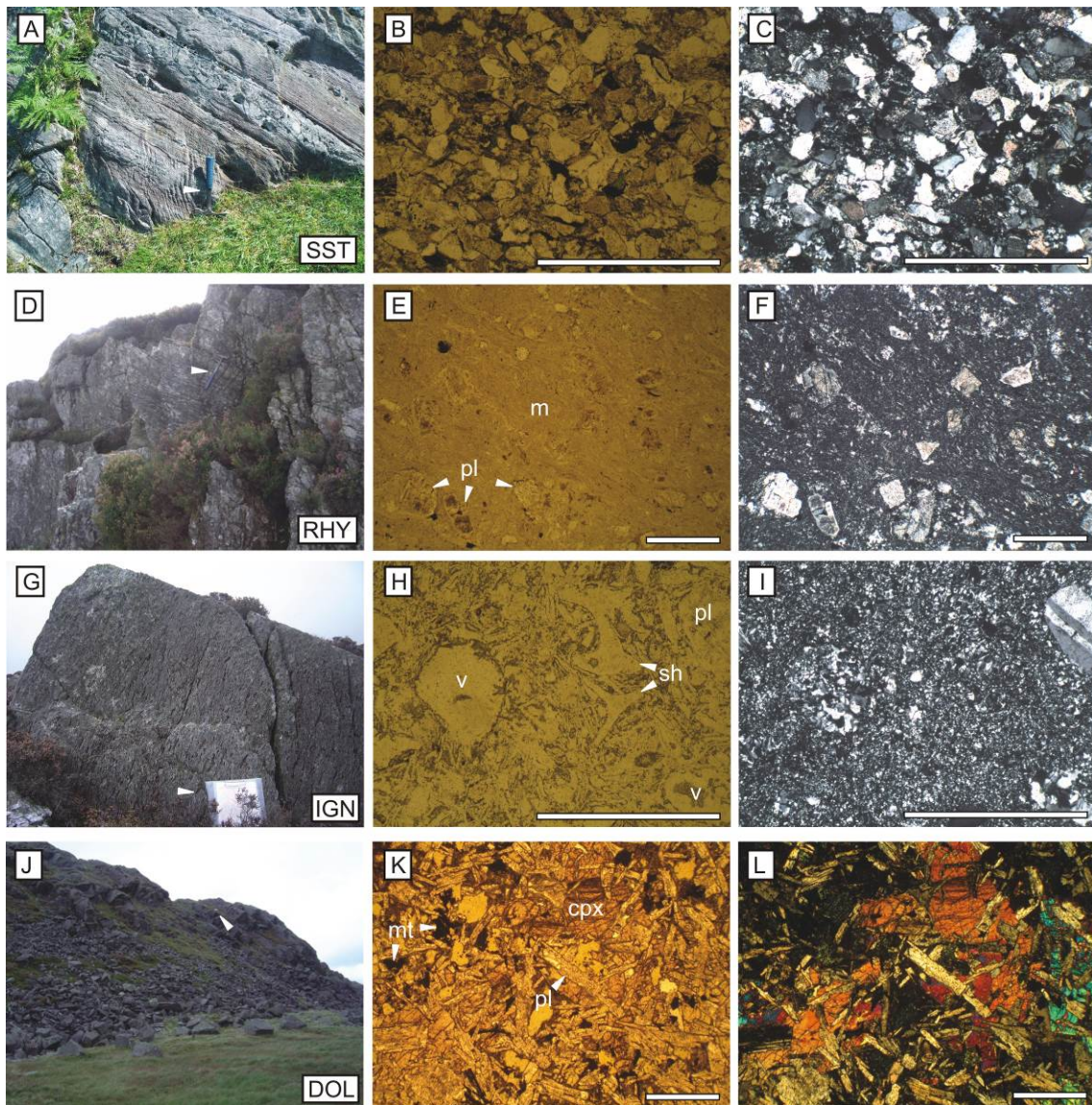
70 **Geological background**

71

72 The geology of the Snowdonia National Park in North Wales comprises a thick
73 sequence of Lower Palaeozoic shallow marine sediments, acidic igneous rocks
74 and basic intrusions of the Welsh Basin. The sediments comprise mudstones,
75 siltstones, sandstones and volcanic tuffs of both the Cwm Eigiau Formation and
76 Nant Ffrancon Subgroup (**Fig. 2**) and typically contain mono-mineralic quartz
77 assemblages (**Fig. 3A-C**). Igneous activity was associated with a marginal
78 basin that developed on the Avalonia continental terrane as a result of
79 subduction and closure of the Iapetus Ocean at ~450 Ma. Igneous activity is
80 characterised by both basic and acidic igneous rocks, with the latter consisting
81 of rhyolitic lavas and, in some cases, thin sheet-like intrusions, dominated by
82 quartz and alkali feldspar (**Fig. 3D-F**), with volcanoclastic ignimbrites deposits
83 (**Fig. 3G-I**). These igneous units are from the Lower Rhyolitic Tuff and
84 Penmaen Tuff Formations (**Fig. 2**) of the Snowdon Volcanic Group. The rocks
85 are cut by a number of later Ordovician sheet-like basic dolerite intrusions (**Fig.**
86 **2**), which consist of clinopyroxene, plagioclase feldspar and magnetite (**Fig. 3J-**
87 **L**). Post-depositional Caledonian Orogeny tectonic processes led to
88 widespread structural deformation. This major tectonic event developed
89 cleavage, tectonic joints, regional low-grade (sub-greenschist) metamorphism
90 and large-scale faulting and folding (*cf.* **Fig. 2**). Subsequent Quaternary
91 glaciations have varied the quality and extent of rock outcrops (**Fig. 4**). Glacial
92 deposition is primarily responsible for outcrop cover, burying the basic dolerite
93 intrusion that forms a major geophysical target here.



96 **Fig 2.** Geology of the southern Snowdonia area. (A) Local geology (see key)
 97 and study area (red box). (B) Schematic cross-section with position marked in
 98 (A). Modified from British Geological Survey (BGS) Sheet 119 (1997).



100

101 **Fig. 3.** Main rocks (left) with thin sections in plane-polarised (middle) and cross-
 102 polarised (right) light. (A-C) Medium-bedded quartz-rich sandstone; (D-F) Flow-
 103 banded rhyolite with phenocrysts (ph) of quartz and alkali feldspar in fine-
 104 grained matrix (m); (G-I) Devitrified acidic (rhyolitic) volcanoclastic ignimbrite
 105 deposits with characteristic eutaxitic texture (G). Thin sections show vesicles
 106 (v), y-shaped (originally glassy) bubble-wall fragments/shards (sh) and crystals
 107 of plagioclase feldspar (pl); (J-L) columnar-jointed dolerite containing
 108 plagioclase feldspar (pl), clinopyroxene (cpx) and magnetite (mt). Geological
 109 field hammers (arrows) for scale with thin section 1mm scale bars.

110 **Methodology**

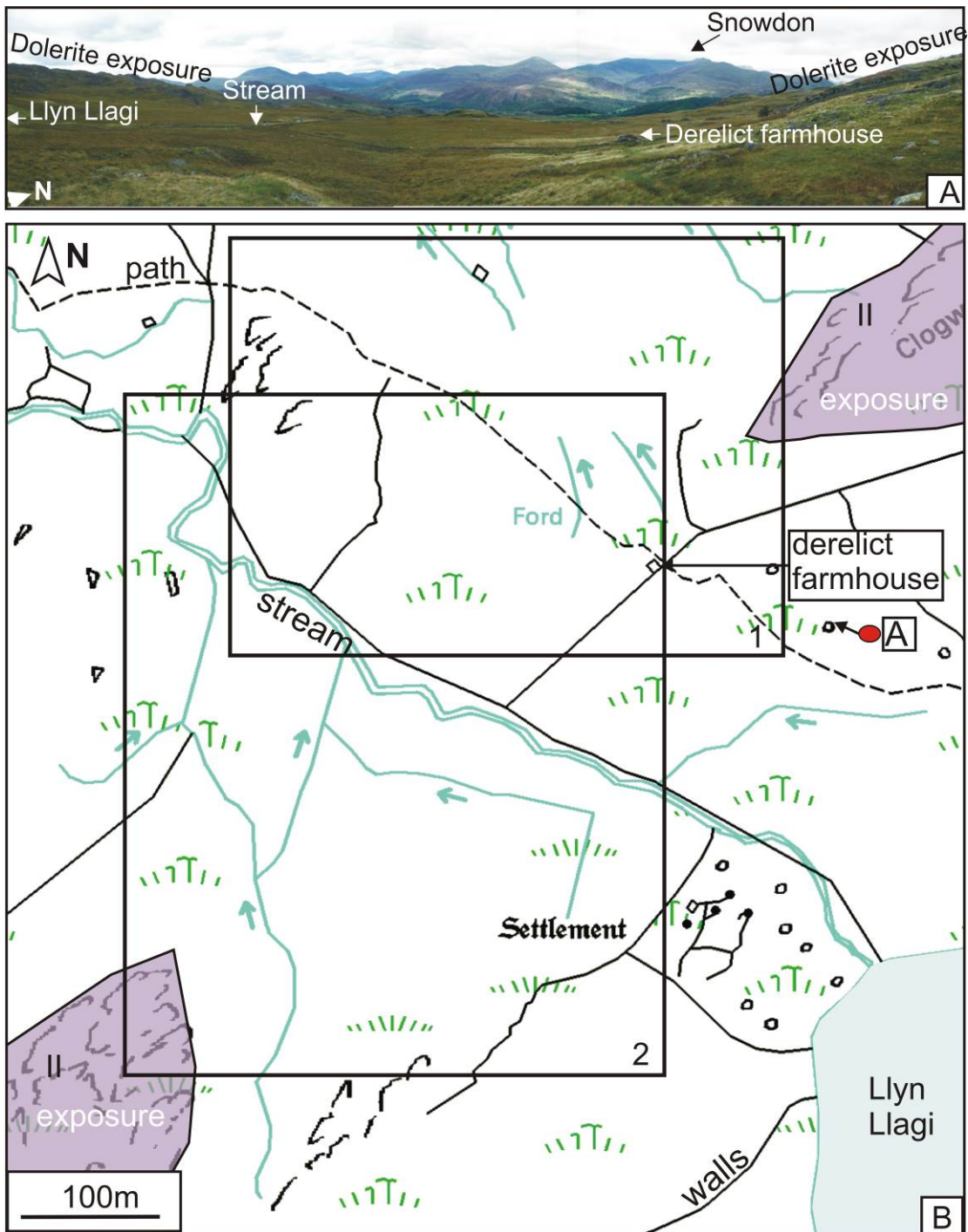
111

112 The study area (**Figs. 2a** and **4**) was geologically mapped over 10 days,
113 identifying and locating rock exposures and lithological boundaries, with major
114 rock type hand specimens collected for thin section analysis (**Fig. 3**). Structural
115 data, including cleavage, bedding and fault plane locations, were also obtained
116 to allow the structural reconstruction of the area (**Fig. 2b**) and aid interpretations
117 of geophysical datasets. To obtain magnetic susceptibility measurements of the
118 main rock types, specimens were used to create $\sim 1 \text{ cm}^3$ cylindrical 10g
119 samples. Samples were placed within a Bartington™ MS2B calibrated (1%)
120 dual frequency sensor and each measured 12 times to gain mean and error
121 bounds (typically less than $\pm 2.5\%$).

122

123 Recent Quaternary sediments that overlay bedrock geology were a mixture of
124 glacially-derived local erratic rocks up to 1 m in diameter and gravel-sized
125 debris down to fine sands and silts. There was also a significant stream running
126 west in the middle of the study area, sourced from Llyn Llagi, a lake to the
127 southeast (**Fig. 4**), and was an obvious source of stream-derived sediments.

128



129

130 **Fig. 4.** (A) Photomosaic of study area (foreground) showing recent deposits
 131 burying bedrock geology, with Snowdon in background. (B) Study areas
 132 showing exposed outcrop and buried geology.

133

134 Digital aerial photographs of the survey area were ortho-rectified and digitally
135 overlain onto topographic maps to identify outcrop positions, confirm any
136 structural trends identified from ground mapping and recognise lineations not
137 identified at outcrop. Potential buried outcrop locations were also recognised.

138

139 An Elsec™ 825 total field proton precession magnetometer collected fourteen
140 2D profiles over three days, using 10 m sampling spacing where possible.
141 Each sample point had a minimum of three readings acquired, with up to five
142 recorded if there was a large variability observed in the readings. 2D profiles
143 were orientated perpendicular to the presumed dolerite, based on geological
144 and remote sensing mapping data.

145

146 A Very Low Frequency (VLF) conductivity Geonics™ EM-16 receiver instrument
147 with 24 KHz (Maine, US source transmitter) obtained local EM field vector
148 angles at ~10 m spaced sample locations on the same 2D profiles. VLF data
149 are not usually collected in the UK as the transmitter at Rugby has been
150 switched off. For each sample position, the instrument was orientated first
151 horizontally and then vertically to gain null positions sensed using an audio
152 signal, before the vector angle was recorded. A second EM conductivity survey
153 was collected using a Geonics™ EM-31 Mark-2 instrument, used in Vertical
154 Magnetic Dipole mode and with GPS locationing. Both the inphase and
155 apparent conductivity measurements were recorded at ~3 m intervals.

156

157 Magnetic and EM-31 datasets were processed by; (1) data 'de-spiking' to
158 remove anomalous data points using a ± 2 SD filter; (2) diurnal correction
159 (magnetics); (3) detrending to remove long wavelength site effects; (4) profile
160 average adjustment to match cross-line measurements and; (5) importing into
161 software and linear gridding to best-fit a digital surface.

162

163 **Survey Results**

164

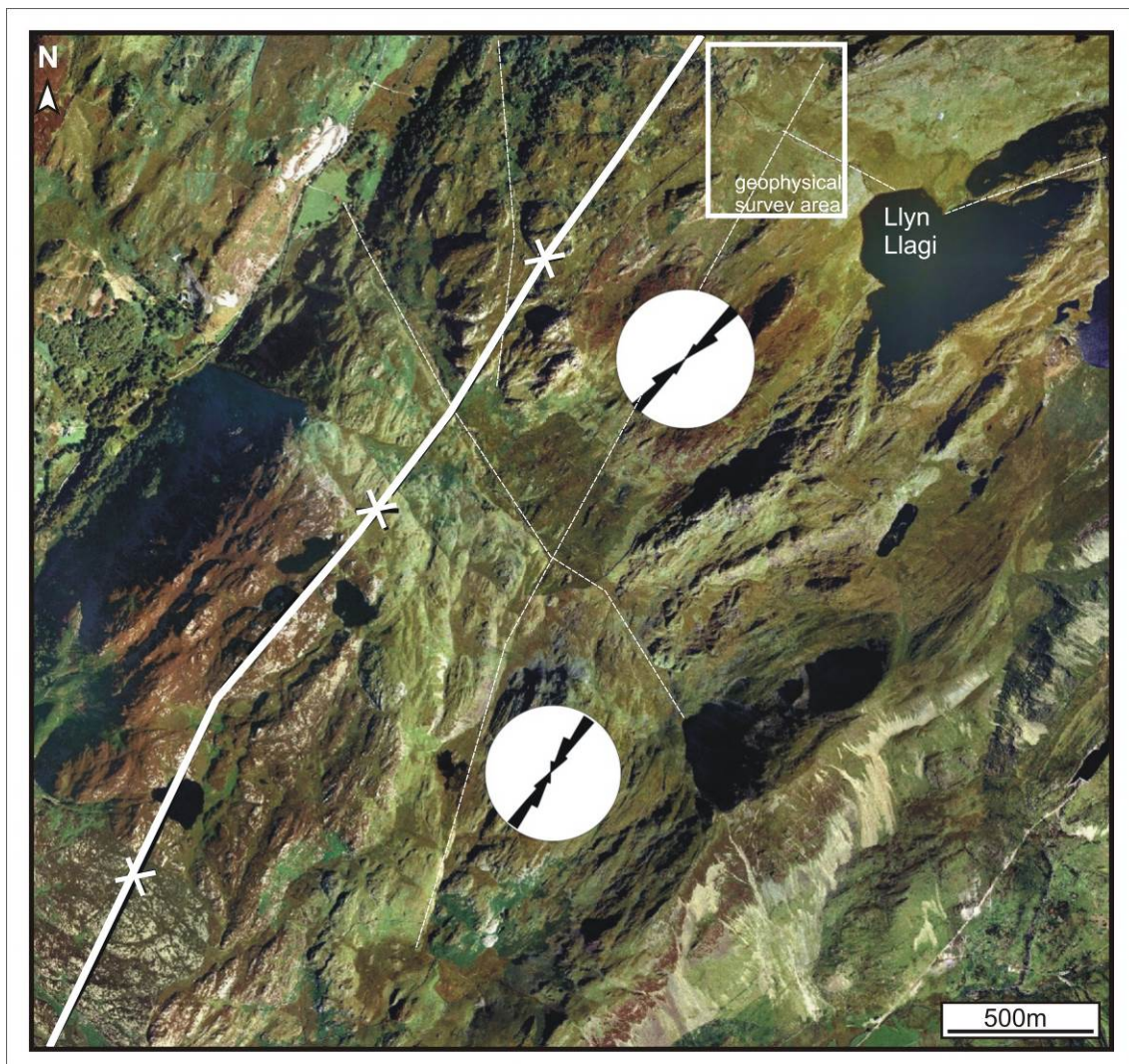
165 Geological field mapping located and identified the main rock types in the study
166 area. A spatially extensive but laterally thin dolerite intrusion was identified
167 intruding through older sedimentary units with a northeast-southwest trend;
168 however this could not be observed due to recent burial. Thin section analysis
169 showed the sandstone rocks contained well sorted mono-mineralic quartz
170 assemblages. In contrast, the dolerite intrusion consists of clinopyroxene,
171 plagioclase feldspar and, importantly, an iron-bearing mineral (magnetite). All
172 lithologies had the chlorite mineral present, consistent with regional, low-grade
173 metamorphism.

174

175 The rock sample magnetic susceptibility measurements ranged from 214.3 e^{-6} –
176 222.9 e^{-6} S.I. in the sandstone to 410.3 e^{-6} to 418.0 e^{-6} in the target dolerite,
177 indicating a geophysically mappable relative magnetic susceptibility contrast of
178 at least 200 e^{-6} S.I.

179

180 Aerial photograph interpretation identified several poorly exposed outcrops
181 which were investigated. Structural interpretation identified several small faults
182 that may have displaced the target dolerite intrusion. An extensive lineation to
183 the southwest was interpreted to be a strike-slip fault orientated, supported by
184 abundant field quartz mineralisation (**Fig. 5**). Several other interpreted faults
185 corresponded to the regional northwest-southeast Caledonian trend.



186
187 **Fig. 5.** Remote sensing image (study area marked), with interpreted faults
188 (dotted lines) and summary structural trend rose diagrams. The major Yr Arddu
189 structural syncline axis position also marked (white line).

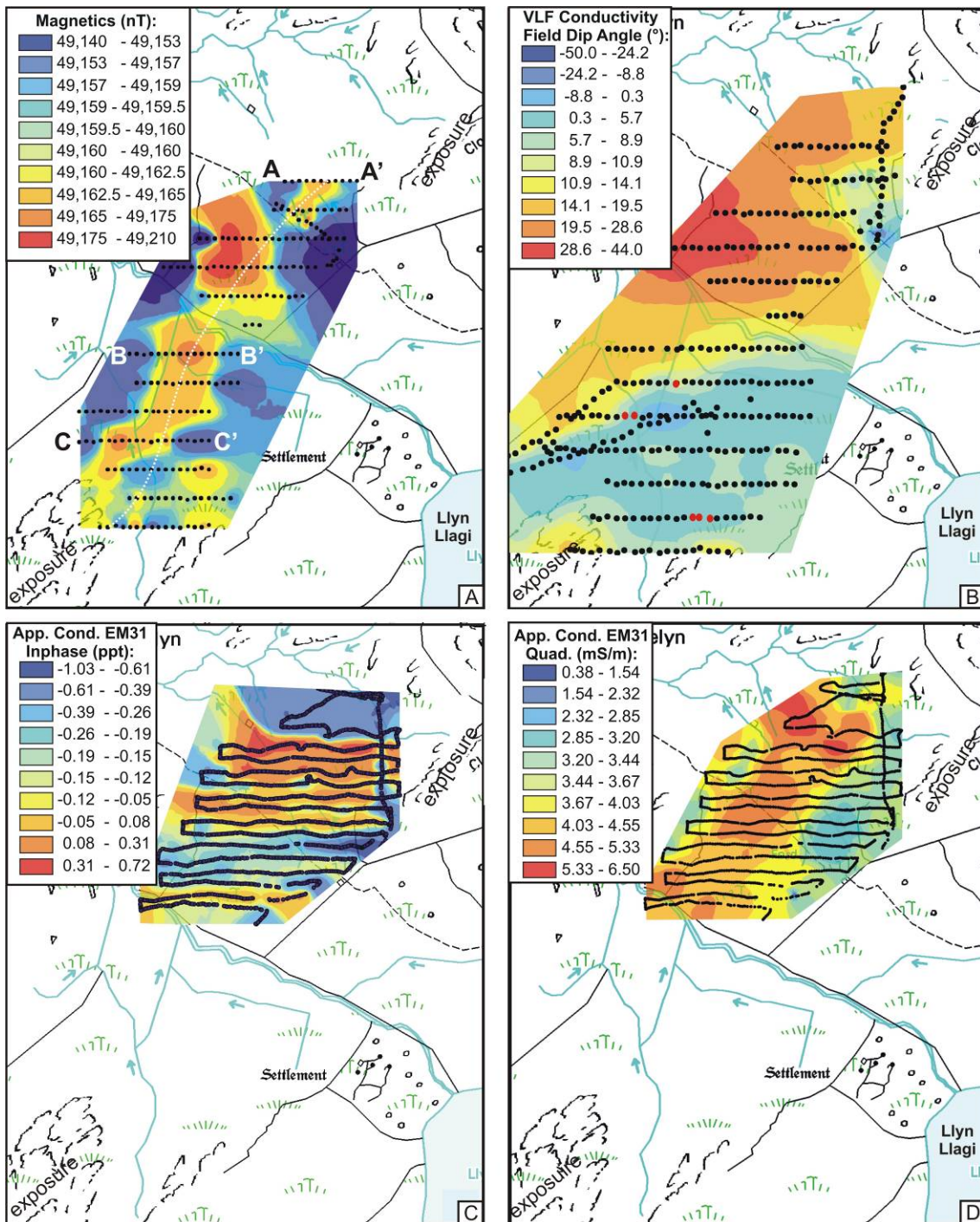
190

191 The magnetic dataset had a well defined, northeast-southwest trending, area of
192 relatively high magnetism, with respect to background values, in the centre of
193 the study area (**Fig. 6a** and **7a**). Total field intensity measurements ranged
194 from 49,140 nT to 49, 210 nT. Determining the overlying drift deposits'
195 thickness was difficult as anomaly amplitudes were variable between profiles, ~
196 4 nT to ~ 60 nT higher than background.

197

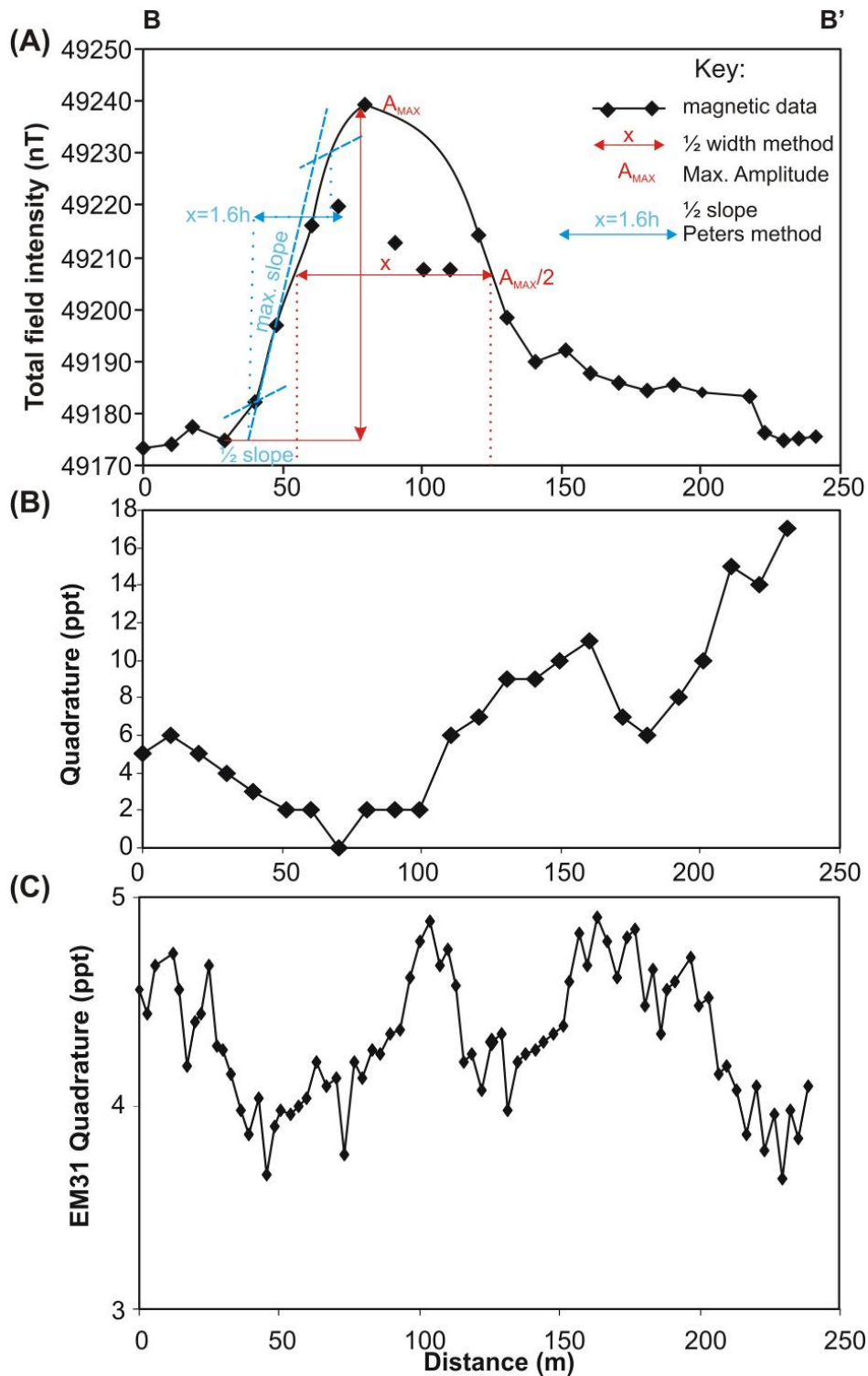
198 The VLF vector field dataset showed overall high vector positive angles to the
199 north and extreme south and relatively low vector negative angles to the south-
200 central part of the study area (**Fig. 6b**). This suggests that the conductivity
201 anomaly was orientated east-west. Qualitative analysis of 0° dip angle
202 locations on 2D profiles, commonly used in VLF surveys to indicate target
203 positions, did not show an obvious correlation between profiles (**Figs. 6b** and
204 **7b**). The apparent conductivity EM-31 inphase dataset showed a general area
205 of high conductivity in the centre of the study area (**Fig. 6c**). The EM-31
206 quadrature dataset showed a fairly well-defined, northeast-southwest aligned
207 area of high conductivity located in the centre (**Figs. 6d** and **7c**). EM-31
208 apparent conductivity quadrature values ranged from 0.38 mS/m to 6.5 mS/m
209 with the highest recorded values located towards the north.

210



211

212 **Fig. 6.** (A-D) Colour contoured (see respective keys) geophysical maps of total
 213 field magnetic, VLF and bulk ground conductivity EM-31 surveys. Black dots
 214 are sampling positions. B – B' shows Fig. 7 geophysical profile. In (C) red dots
 215 indicate 0° VLF field vectors.



216

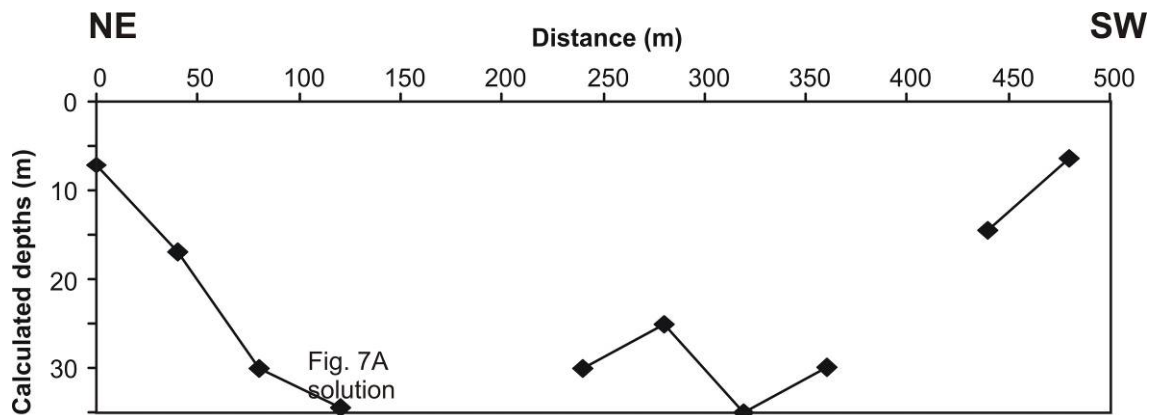
217 **Fig. 7.** 2D profile B comparison of geophysical data (Fig. 6B for location); (A)
 218 magnetics; (B) VLF and (C) EM-31 bulk ground surveys. (A) graphically
 219 illustrates target depth 1/2 width (red) and Peters half-slope (blue) estimation
 220 methods; calculated depths of ~35 m and ~65 m on this profile.

221 **Target depth estimation**

222

223 Simple graphical analysis of geophysical anomaly relative shapes and
224 amplitudes can be used to determine target depth(s) and orientation(s). The
225 half-width and Peters half-slope methods were used on magnetic profiles (see
226 **Fig. 7A**); but target depth estimates were quite variable, between ~7 m to ~75
227 m on eleven of the fourteen profiles. The half-width method does not work
228 when the target is not symmetrical or vertical; therefore the half-slope method
229 was used to calculate target depths, generating a NE-SW trending transect
230 across the study area (**Fig. 8**). Whilst useful, these target depth estimation
231 methods can have a 30% measurement error with depths in the centre also
232 being quite variable.

233



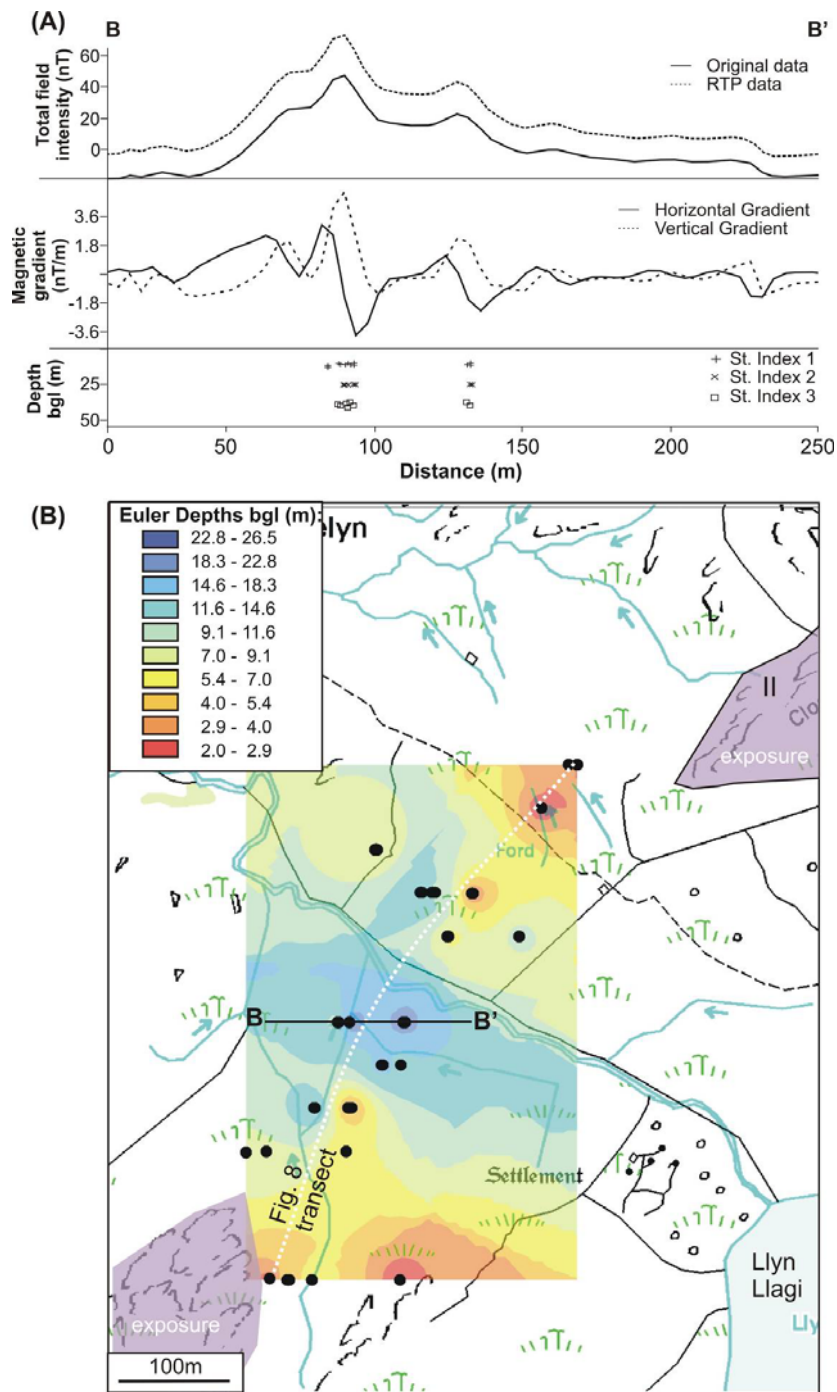
234

235 **Fig. 8.** Calculated target depths transect across the study area (Fig. 6B for
236 location). These solutions based on Peters' ½ slope method on 2D magnetic
237 profile anomalies (Fig.7A solution marked).

238

239 Euler deconvolution provides numerical solutions for bodies causing
240 geophysical anomaly relative shapes and amplitudes using a structural index.
241 2D magnetic profile data were analysed using this method using structural index
242 1, a vertical tabular body best estimating the target. This is quantitative,
243 corrects for the Earth's magnetic field and gives clusters of structural solutions
244 and target depths (**Fig. 9a**). Euler deconvolution depth solutions varied from 2
245 m – 27 m with a 10 m average across the study area, their spatial positions
246 merged into a single dataset to create a best-fit digitally contoured surface.
247 This (**Fig. 9b**) showed a similar trend to Peters' $\frac{1}{2}$ slope method calculations but
248 were less variable and generally shallower. The deepest target depth mirrored
249 both the orientation of the stream and a local fault (*c.f.* Figs. 5 and 9b).

250



251

252 **Fig. 9.** (A) Euler deconvolution on 2D magnetic profile B (Fig. 6B for location).
 253 (top) original data and reduced to magnetic pole (RTP); (middle) horizontal and
 254 vertical gradient and (bottom) euler deconvolution solution for structural indices
 255 1-3 (see text). (B) Colour contoured bedrock depth using euler deconvolution
 256 structural index 1 solutions (black dots).

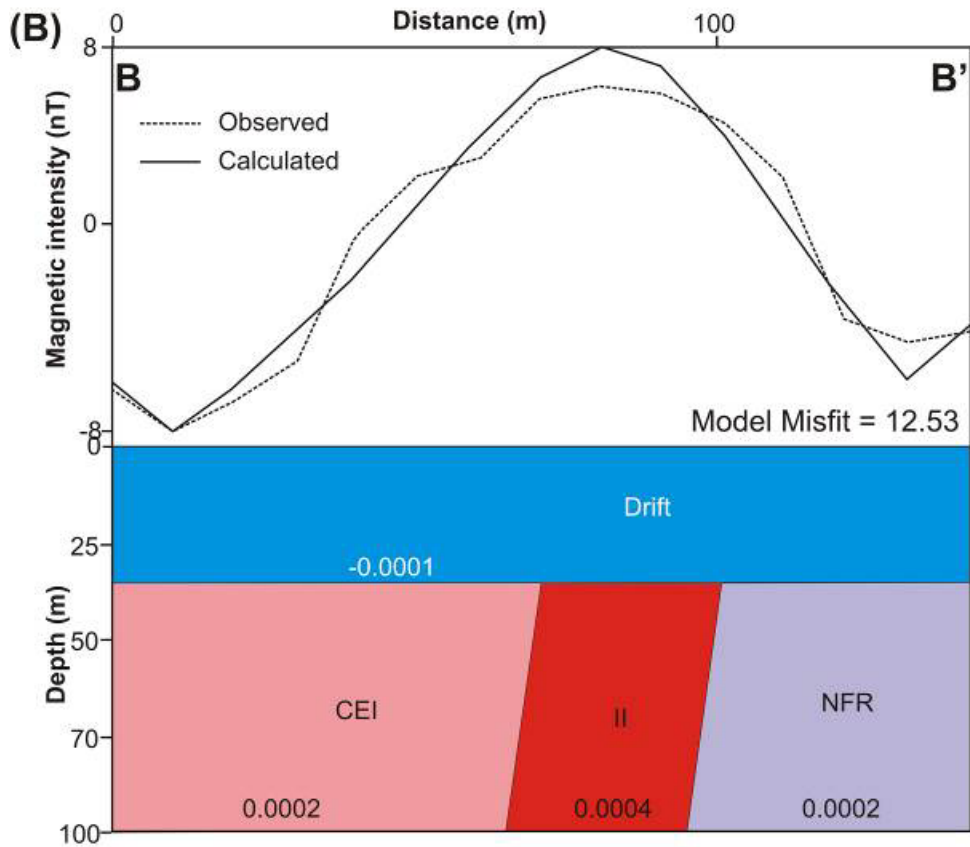
257 **2D Numerical modelling**

258

259 Numerical modelling can determine buried target(s) depths and widths by
260 creating models of buried layer(s) and/or object(s) with geometries and relative
261 values. A calculated magnetic profile can be generated by combining modelled
262 body values, also adjusting for local geophysical fields and profile orientations.
263 The calculated profile can then be quantitatively compared with field-collected
264 data; any resulting mis-fit can be analysed and reduced by either changing the
265 modelled body values and/or modelled body geometries and spatial positioning.

266

267 2D depth models were generated for twelve profiles using geology information,
268 rock sample magnetic susceptibility measurements and Euler deconvolution
269 solutions. These profiles were calibrated to observed data and misfits reduced
270 by only varying target intrusion body width and drift geology body geometries
271 (**Fig. 10**). Model mis-fits were small (12.7 to 67.5 with a 33.5 average), which
272 gave confidence that models were reasonable. The modelled target dolerite
273 width was variable (10 – 60 m with a 28.6 m average), with two intrusions
274 needing to be modelled in the south. Spatial positions of modelled target
275 intrusions were transferred onto a study site map, together with Euler
276 deconvolution solution locations for comparison (**Fig. 11**).



277

278 **Fig. 10.** 2D magnetic numerical model of profile B (position in Fig. 6B). (top)
 279 Observed and model-calculated magnetic data and (bottom) 2D model with rock
 280 (Fig.2 for key) body geometries and magnetic susceptibility values.

281

282 **Discussion**

283

284 The use of geological mapping combined with remote sensing can construct
 285 basic geological maps of a study area. Ground-based near-surface geophysics,
 286 particularly magnetics, can detect buried highly ferromagnetic geological
 287 targets, based on higher magnetic and bulk ground conductivity values.

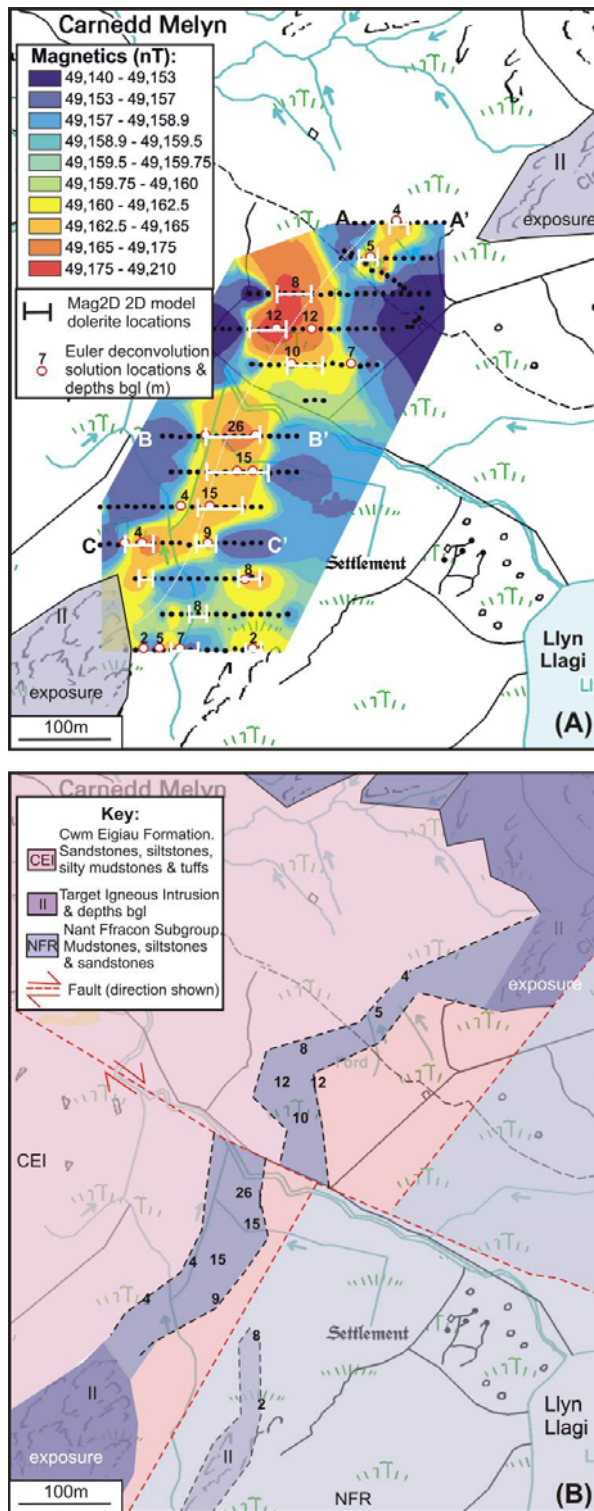
288 Laboratory magnetic susceptibility measurements of field rock samples also

289 gave confidence in geophysical findings. Qualitative analysis of the EM VLF
290 dataset showed an approximately east-west orientated feature correlated with a
291 suspected fault zone. Magnetic surveys were good quality and analysed using
292 simple graphical methods of 2D magnetic profiles. Euler deconvolution
293 solutions gave more quantitative target depths that showed a similar geometry
294 transect but were less variable and significantly shallower (averages of ~10 m
295 for Euler versus ~23 m for Peters half-slope method respectively). Numerical
296 modelling created models calibrated by outcrop and remote sensing, magnetic
297 profile field data, rock sample magnetic susceptibility measurements and Euler
298 deconvolution solutions. Relatively small mis-fits between model-calculated
299 magnetic profiles and collected magnetic datasets were generated by
300 numerically varying the target body width and superficial deposit thicknesses..

301

302 Combining all datasets allowed an accurate geological map to be created (**Fig.**
303 **11b**), which would not have been possible without integration of near-surface
304 geophysical datasets, and their detailed analysis described in this study. The
305 magnetic survey was deemed crucial to not only locate and map the target
306 igneous intrusion, but also to allow depth estimates to be quantitatively
307 estimated. This detailed analysis went beyond conventional survey
308 methodologies and also allowed the location of later structural displacements,
309 namely linear strike-slip faults with typical Caledonian Orogeny orientations, to
310 be suggested to best-fit the datasets.

311



312

313 **Fig. 11.** (A) Summary map of target dolerite intrusion from numerical models.

314 Fig. 6B contoured magnetic data underlayed. Euler deconvolution locations

315 and calculated depths also shown. (B) Summary map, numbers indicating

316 target depths and with a offsetting fault present.

317 **Conclusions**

318

319 Detailed geological mapping, remote sensing and near-surface geophysics
320 were all combined to generate a detailed geological map. Total field
321 magnetometer surveys were critical in determining a buried target dolerite sheet
322 intrusion. The EM VLF technique detected a east-west orientated conductive
323 structural feature. Simple graphical analysis of magnetic anomalies was shown
324 to delineate bedrock depth but quantitative Euler deconvolution solutions of
325 magnetic anomalies were most accurate which was, on average, ~13 m
326 shallower than graphical analysis results. Finally 2D numerical modelling
327 confirmed the depth of overburden. The final geological map generated agrees
328 with the generally agreed geological evolution of the area.

329

330 **Further reading:**

331

332 Howells M.F. and Smith M. 1997. *Geology of the country around Snowdon. The*
333 *Stationery Office*, London.

334 Lisle R., Brabham P. and Barnes J. 2011. *Basic Geological Mapping. The*
335 *Geological Field Guide Series*, John Wiley and Sons Ltd., 5th Edition.

336 Milsom J. and Eriksen A. 2011. *Field Geophysics. The Geological Field Guide*
337 *Series: 4th Edition*. Wiley.

- 338 Murdie R.E., Styles P., Upton P., Eardley P. and Cassidy N.J. 1999. Euler
339 deconvolution methods used to determine the depth to archaeological features.
340 In: Pollard A.M. (ed.) *Geoarchaeology: exploration, environments, resources*.
341 *Geological Society of London Special Publication* **165**, 35-40.
- 342 Pringle J.K., Cassidy N.J., Styles P., Stimpson I.G. and Toon S.M. 2010.
343 Training the next generation of near-surface geophysicists: team-based
344 student-led, problem-solving field exercises, Cumbria, U.K. *Near Surface*
345 *Geophysics* **8**, 503-517.
- 346 Reynolds J.M. 2011. *An Introduction to Applied and Environmental Geophysics*.
347 2nd Edition. Wiley.
- 348 Schofield D. 2009. What's in the Welsh Basin?: insights into the evolution of
349 Central Wales and the Welsh Borderlands during the Lower Palaeozoic.
350 *Proceedings of the Shropshire Geological Society* **14**, 1-17.